engineering proceedings

MDPI

Proceeding Paper

Geometrical Effects on the Structural Behavior of Octahedral Unit Cells in Anisogrid Sandwich Panels †

Emanuele Vincenzo Arcieri * and Sergio Baragetti

Department of Management, Information and Production Engineering, University of Bergamo, 24044 Dalmine, Italy; sergio.baragetti@unibg.it

* Correspondence: emanuelevincenzo.arcieri@unibg.it

† Presented at the 54th Conference of the Italian Scientific Society of Mechanical Engineering Design (AIAS 2025), Florence, Italy, 3–6 September 2025.

Abstract

Anisogrid lattice structures are gaining increasing attention due to their high strength-to-weight ratios, which make them ideal for the production of lightweight mechanical components. This study presents a finite element model developed to evaluate stress distribution in an anisogrid sandwich panel with an octahedral core. The Taguchi method and analysis of variance (ANOVA) were employed to identify the geometric parameters that mostly influence the stress state and, consequently, the structural strength. The radius of the inclined ribs and the thickness of the skins were identified as the most critical factors, while the influence of the horizontal rib cross-sectional area was found to be minimal. The stiffness and strain energy of different cell geometries were also evaluated, and the results are consistent with the stress-based analysis. These findings offer valuable guidance for optimizing anisogrid geometry, improving load-bearing performance and advancing the design of high-efficiency structures.

Keywords: anisogrid lattice structures; stress; stiffness; strain energy; FEM; Taguchi; ANOVA

1. Introduction

Anisogrid lattice structures have recently garnered significant attention due to their remarkable structural efficiency, which makes them particularly suitable for aerospace applications, where high strength-to-density ratios are essential. These structures consist of ribs periodically arranged in a grid pattern and their fabrication has become increasingly feasible thanks to the rapid advancement of additive manufacturing technologies, which enable rapid and cost-effective production. The exceptional structural, electromagnetic and heat transfer properties of anisogrid lattice structures are mainly due to the engineered geometry of their elementary cell [1–3]. The grid structure enables optimized and efficient internal load redistribution, significantly enhancing buckling resistance and the capability of absorbing large strain energies under compressive loads [4,5].

Totaro and Gürdal [6] proposed an optimization strategy for composite lattice shell structures that targets mass reduction while satisfying buckling, strength and stiffness constraints. Gentili et al. [7] investigated the buckling behavior of anisogrid structures made from carbon fiber reinforced thermoplastics. They found that variations in rib geometry significantly influence their compressive strength and also specific strength. Jeon et al. [8] examined the compressive failure behavior of an anisogrid cylindrical composite lattice structure, considering the effect of manufacturing defects through experimental testing

Academic Editors: Nicola Bonora, Umberto Galietti, Luigi Bruno, Davide Castagnetti, Cristiana Del Prete, Mario Guagliano and Vigilio Fontanari

Published: 30 March 2026

and progressive damage modeling. Structural analysis and optimization methods for cylindrical and conical anisogrid composite lattice shells have been presented in [9,10], using discrete buckling evaluation and parametric finite element modeling to identify mass-efficient designs. Sun et al. [11] conducted a theoretical study to predict failure loads and modes of composite anisogrid lattice sandwich cylinders. They introduced failure mode maps, validated by finite element corrections, which can be used as practical design tools to link structural behavior to geometrical parameters.

Sandwich structures, composed of two skins enclosing a lattice core, offer notable advantages in terms of fluid impermeability and mechanical strength. In a sandwich structure, the outer panels bear external loads, while the internal ribs enhance overall stiffness [12]. In the literature, various studies have investigated the structural performance of sandwich panels. For instance, Li et al. [13] found that tetrahedral sandwich plates with aluminum foam core are effective in absorbing impact energy. Further investigation by Xue et al. [14] examined how skin thickness influences underwater shock resistance in pyramid lattice configurations. Hou et al. [15] compared lattice composites under impact loading, revealing that re-entrant honeycomb cores, despite their lower energy absorption capability, offer superior durability, force mitigation and consistent multi-impact performance due to their compliant deformation and reduced stress concentration. Lei et al. [16] evaluated the mechanical performance and energy absorption capacity of multi-layer lattice sandwich panels with geometrical imperfections using a finite element model that accounts for their specific non-uniform distribution. They found that increasing the number of layers enhances crash efficiency but reduces specific energy absorption due to boundary condition effects and varying failure modes.

The objective of this study is to investigate how the geometry of a single unit cell of an anisogrid sandwich panel made of AlSi10Mg aluminum alloy influences its structural behavior. The single unit cell occupies a volume of 10 mm × 10 mm × 17 mm (b × h × s) and consists of two planar skins and a core composed of ribs arranged in an octahedral lattice structure. The octahedral geometry was chosen for the core due to its favorable crashworthiness performance [17]. The influence of the geometrical parameters was studied by applying the Taguchi method and analysis of variance (ANOVA) to the finite element stress distributions reported in [18]. The radius of the inclined ribs and the thickness of the skins are the most significant parameters, while the influence of the horizontal ribs is minimal. This result is also confirmed by the analysis of the global stiffness and strain energy, providing guidance for designers to improve structural load-bearing capabilities and support the development of high-efficiency components.

2. Materials and Methods

2.1. Taguchi Analysis and ANOVA

The Taguchi method [19] provides a rapid and effective approach for evaluating the geometrical parameters of the elementary cell of the sandwich panel which mostly influence the stress distribution. It also enables the identification of the optimal parameter levels to minimize stresses and thereby enhance structural strength. An L9(3^4) Taguchi array was used to determine how to vary the input parameters. This array allows examination of the effect of four parameters with three levels through only nine runs. The analyzed geometrical parameters are the radius of the inclined ribs r_{incl}, the radius of the horizontal ribs r_{hor} and the skin thickness t_{skin}. A fourth parameter, named "empty" and undefined, was used to assess whether all the relevant factors influencing the stress distribution in the elementary cell of the sandwich panel were included. The array containing the parameters and their corresponding levels is reported in Table 1.

https://doi.org/10.3390/engproc2026131015

Table 1. Input data for Taguchi analysis [18] according to L9(3^4) Taguchi array [19].

Run	r_{incl} (mm)	r_{hor} (mm)	t_{skin} (mm)	Empty
1	0.250	0.250	1.0	level 1
2	0.250	0.375	1.5	level 2
3	0.250	0.500	2.0	level 3
4	0.375	0.250	1.5	level 3
5	0.375	0.375	2.0	level 1
6	0.375	0.500	1.0	level 2
7	0.500	0.250	2.0	level 2
8	0.500	0.375	1.0	level 3
9	0.500	0.500	1.5	level 1

In the Taguchi method, data dispersion is quantified using the Mean Square Deviation (MSD). Since the aim of this study is to identify the most influential parameters and their optimal levels for minimizing stresses in the elementary cell, the response variable "stress" was evaluated using the "smaller is better" modality, which is appropriate for minimization objectives. Consequently, the MSD is calculated according to Equation (1):

$$\mathrm{MSD} = \left(\frac{\sum_{i=1}^{n} Y_i^2}{n} \right), \tag{1}$$

where Y_i represents the response variable Y (in this work the maximum von Mises stress in the cell was analyzed) obtained from the i-th test of a run and n is the number of tests per run. A single finite element simulation was conducted for each run, due to the deterministic nature of the results; therefore $\mathrm{MSD} = Y^2$.

The other steps of the Taguchi method are as follows:

- Calculation of the signal-to-noise ratio, S/N, that quantifies the position and variability of the observed effect (Equation (2)):

$$\mathrm{S/N} = -10\log(\mathrm{MSD}); \tag{2}$$

- Calculation of the average signal-to-noise ratio, S/N′, for each level of each parameter;
- Calculation of the quantity ΔS/N for each parameter, that is the difference between the maximum and the minimum values of S/N′.

A higher value of ΔS/N indicates a more pronounced influence of the considered parameter on the response. For each parameter, the level associated with the highest S/N′ is the optimal.

ANOVA was employed to determine the percentage contribution of each factor to the total variation and to assess the confidence of the results. For a parameter in an L9(3^4) array, the source variation S_x is defined by Equation (3):

$$S_x = \frac{W_1^2 + W_2^2 + W_3^2}{\frac{n_T}{3}} - \frac{T^2}{n_T}, \tag{3}$$

where W_1, W_2 and W_3 are the sums of the response values for the parameter W at levels 1, 2 and 3 respectively; n_T is the total number of data points, equal to 9 in this study; and T is the sum of all response values. If the variation in a parameter is smaller than that in an empty parameter or significantly lower than that in other parameters, it may be considered random and treated as pooled. The following equations define the quantities used in ANOVA:

https://doi.org/10.3390/engproc2026131015

- Variance of the source corrected for degrees of freedom, V_x (Equation (4)):

$$V_x = S_x/dF, \tag{4}$$

- Variance of pooled parameters, V_e (Equation (5)):

$$V_e = S_e/dF_e, \tag{5}$$

- F-ratio for significant parameters, F (Equation (6)):

$$F = V_x/V_{eTOT}, \tag{6}$$

- Pure variation in the source for significant parameters, S_x^* (Equation (7)):

$$S_x^* = S_x - dF \cdot V_{eTOT}, \tag{7}$$

- Percentage contribution to total variation, ρ% (Equation (8)):

$$\rho\% = S_x^*/S_{xTOT}, \tag{8}$$

where dF is the number of degrees of freedom for each parameter, i.e., the number of parameter levels (3) minus one; S_e is the variation in a pooled parameter; dF_e is the number of degrees of freedom for a pooled parameter; V_{eTOT} is the total error variance; and S_{xTOT} is the total corrected variation for unpooled parameters. The F-test via ANOVA enables the calculation of confidence for the results regarding von Mises stress.

The application of the Taguchi method to the stress state in the elementary cell is presented in Section 3.

2.2. Finite Element Model

The finite element model of the unit cell was developed using Abaqus 2022 software and is schematized in Figure 1 [18]. The core ribs and the skins were modelled with B31 elements and S4R elements, respectively. A mesh size of 0.25 mm was adopted for the entire model, based on the results of a performed mesh convergence analysis. To maintain a constant cell height while varying the skin thickness, the core height was adjusted accordingly. Outward extension of the skins was implemented via section assignment on the shell elements, defining the offset direction to project away from the core (Figure 1a). This allowed for accurate calculation of the inertia properties of the cell. The AlSi10Mg alloy of the cell was modeled as a homogeneous and isotropic material. A linear elastic behavior was assumed, with a Young's modulus E = 70 GPa and a Poisson's ratio ν = 0.34. The centers of the external panels coincide with the ends of the inclined ribs they intersect and establish geometric continuity. However, such a modelling approach may lead to stress concentrations. To more accurately reproduce the load transfer between the skins and the intersecting inclined ribs, the rib ends were connected to square partitions located at the center of the skin surfaces. The edge length of the created partitions was set equal to the diameter of the inclined ribs and the connection was performed using continuum distributing couplings with all rotational degrees of freedom locked (Figure 1b). A static analysis was carried out, with geometric nonlinearity accounted. A uniform pressure was applied on the upper skin, resulting in a force of 50 N (Figure 1c). The edges of the lower panel were fixed.

https://doi.org/10.3390/engproc2026131015

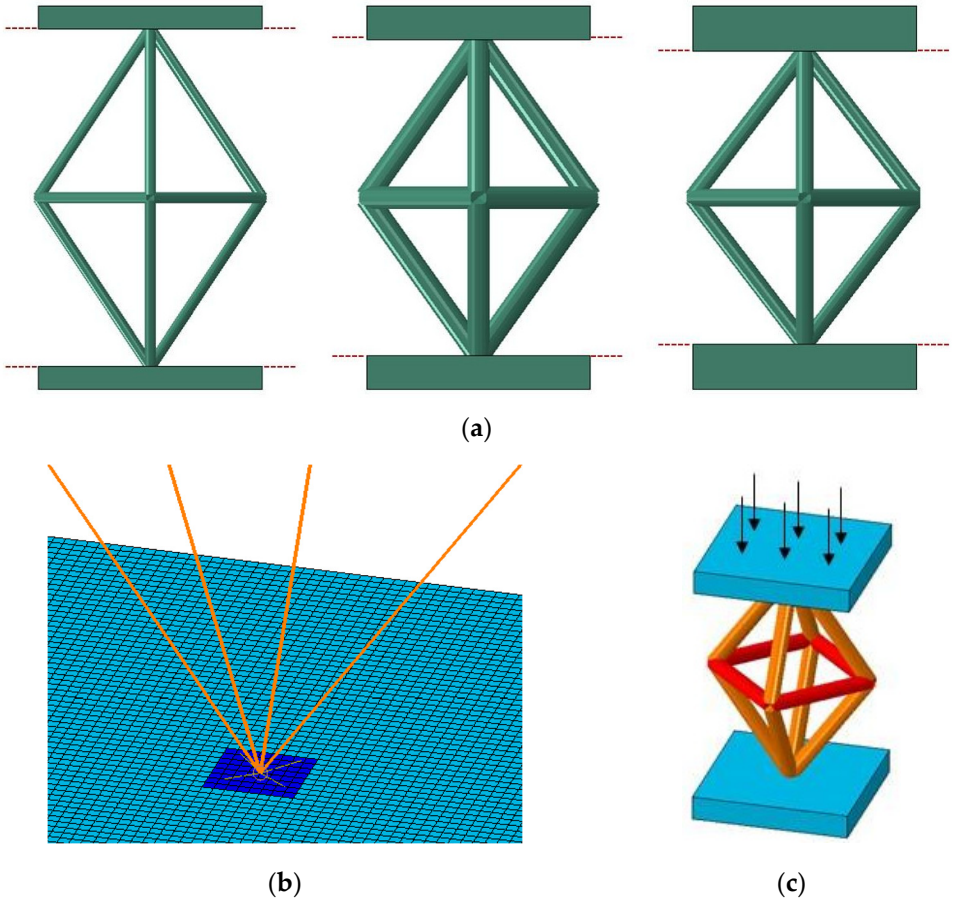

Figure 1. Finite element model: (**a**) Renderings to show the constant height of the simulated cells (the planes of the shell elements are indicated by red lines); (**b**) Modelling of the connection between the skin and the inclined ribs (ribs in orange, square partition in blue, remaining skin in light blue, continuum distributing coupling in yellow); (**c**) Rendering of the unit cell and applied load [18].

3. Results and Discussion

Figure 2 shows the von Mises stress distributions in the elementary cell for the nine runs. The stress values vary considerably depending on the geometric configurations. Run 1 exhibits the highest stress level (93 MPa), while Runs 5 and 9 show the lowest values (35 MPa and 32 MPa), indicating a significant influence of geometric parameters on stress distribution. Moreover, the location of the maximum stress shifts across the cases, further emphasizing the sensitivity of the structure to parameter changes. In Runs 2, 3 and 5, the peak stress occurs in the inclined ribs; the maximum stress is located in the horizontal ribs for Runs 4 and 7; and for Runs 1, 6, 8 and 9, the skins bear the highest stress [18].

The results of the Taguchi method, shown in Table 2, point out the influence of the individual parameters. The optimal parameter levels are underlined in the table to emphasize the optimal configurations identified. Considering the radius of the inclined ribs, the best S/N′ ratio occurs for r_{incl} = 0.500 mm, which is the maximum tested dimension. The ΔS/N of 3.97 suggests this parameter has a strong effect on stress distribution. The ΔS/N value of 1.87 obtained for the radius of the horizontal ribs r_{hor} indicates a moderate influence on stress distribution in the cell. Based on the results, the intermediate value of 0.375 mm yields the highest S/N′ ratio and should be therefore preferred. However, the difference between the S/N′ values for r_{hor} = 0.375 mm and r_{hor} = 0.500 mm is minimal, suggesting that both configurations can be considered optimal. For this reason, both values are underlined in Table 2. Skin thickness t_{skin} also plays a substantial role, with thinner skins (1.0 mm) leading to elevated stress levels and thicker skins (1.5 mm and

2.0 mm) contributing to improved stress distribution. The optimal S/N′ is achieved at the intermediate thickness of 1.5 mm but the difference between S/N′ for t_{skin} = 1.5 mm and t_{skin} = 2.0 mm is very small. Since the Taguchi analysis indicates that the intermediate values of r_{hor} and t_{skin} should be preferred, this finding could be used for a design strategy that reduces the mass of the elementary cell and, by extension, the overall mass of the sandwich panel. The "empty" parameter also emerges as significant for stress variation, with a ΔS/N of 3.93. Its physical meaning is not explicitly defined but it may correspond to factors such as the material composition of the cell, the magnitude of the applied load or additional geometric features like sandwich panel thickness or the overall volume occupied by the cell. The ANOVA results, presented in Table 3, reinforce these findings, highlighting the radius of the inclined ribs r_{incl} as the most influential factor, which contributes 33% to the total variance with a confidence level of 86%. Skin thickness t_{skin} follows, since it has a contribution of 25% with a confidence level of 83%. The "empty" parameter is less dominant and accounts for 16% to the variance with a confidence level of 78%. Further investigation into its nature could provide valuable details into structural performance.

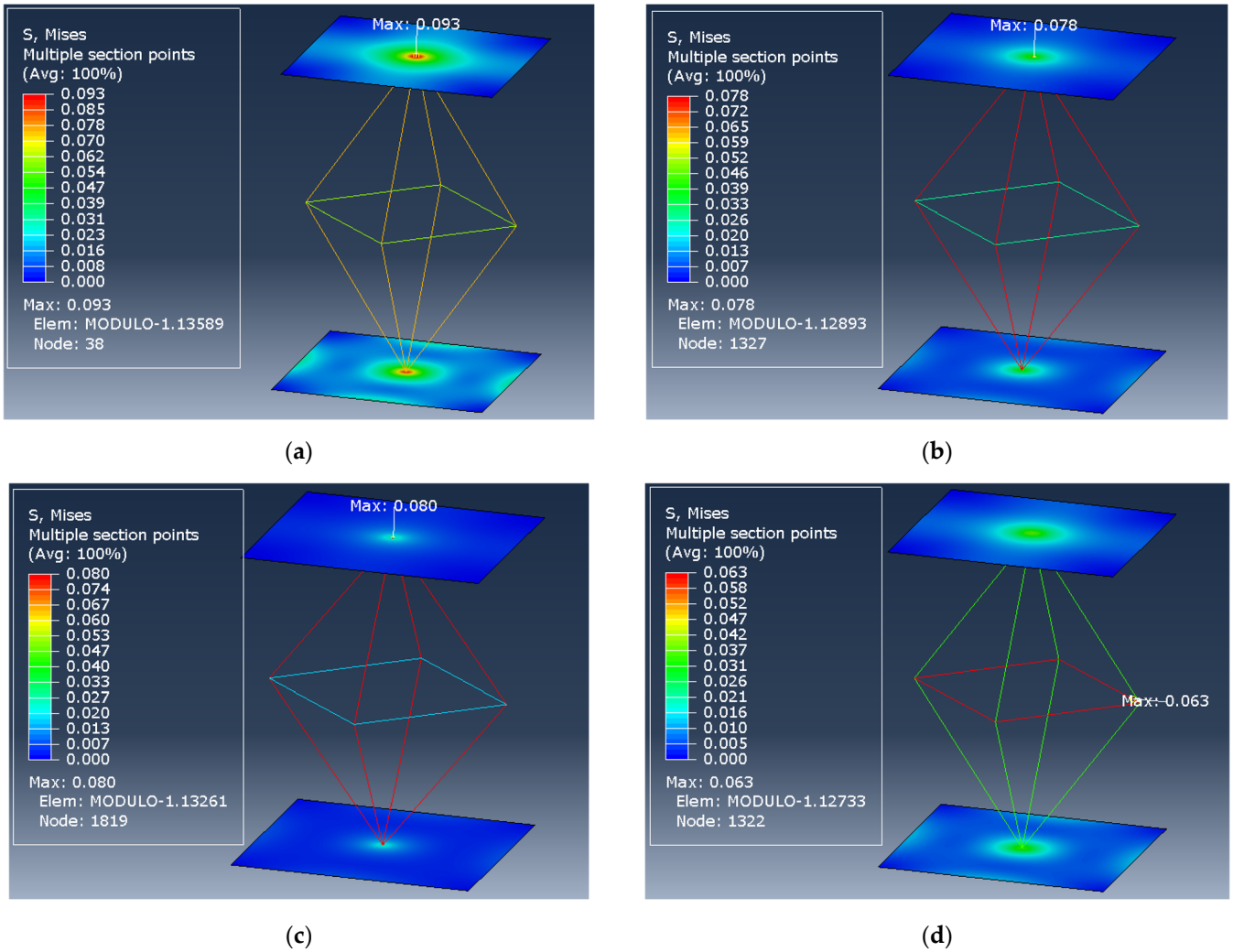

Figure 2. *Cont.*

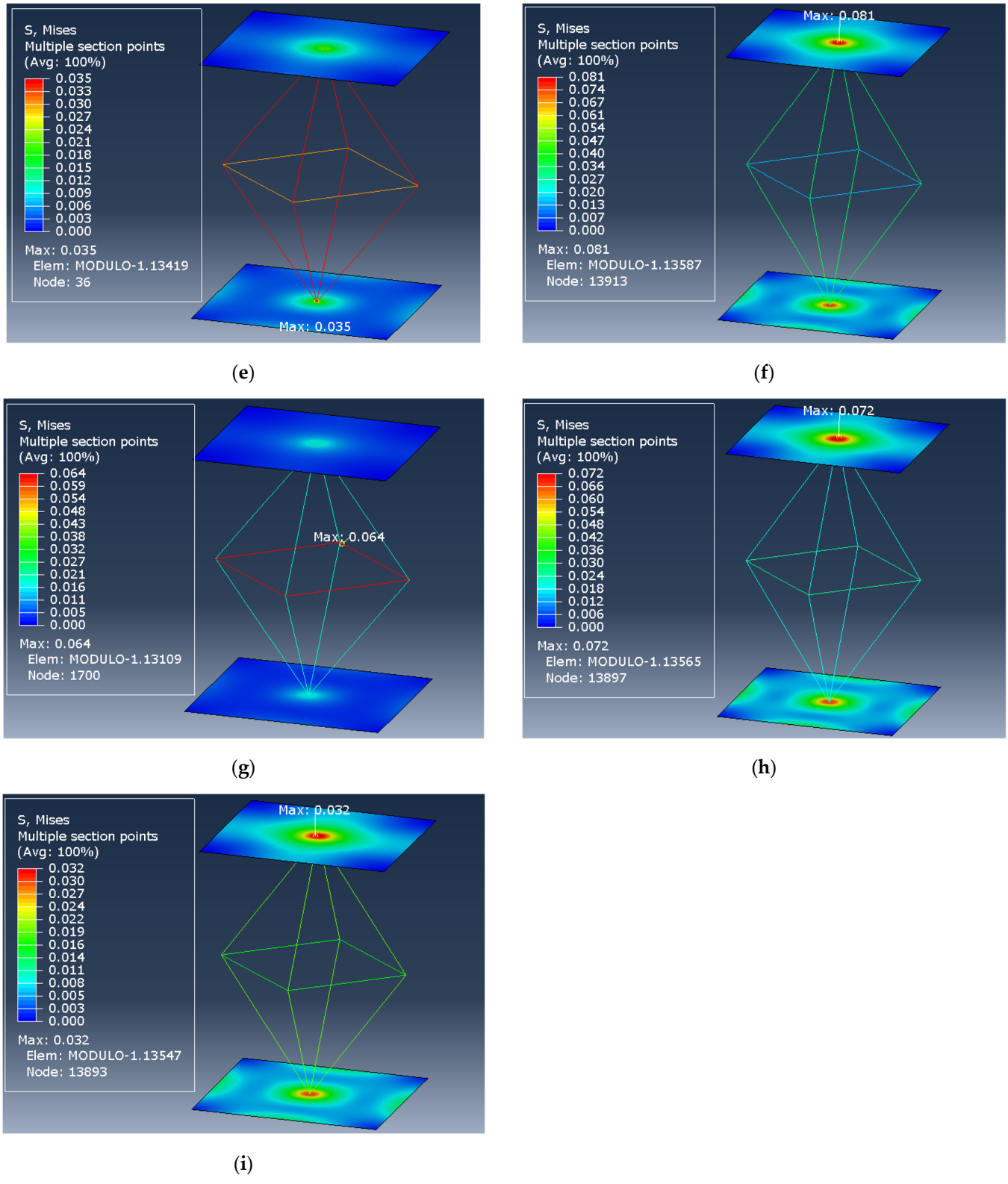

Figure 2. Von Mises stresses (GPa): (**a**) Run 1; (**b**) Run 2; (**c**) Run 3; (**d**) Run 4; (**e**) Run 5; (**f**) Run 6; (**g**) Run 7; (**h**) Run 8; (**i**) Run 9 [18].

Table 2. Results according to the Taguchi method, best parameter levels are underlined.

Run	Y = max(σ_{VM}) (MPa)	MSD	S/N	Parameter	Parameter Level	S/N′	ΔS/N
1	93	8649	−39.37	r_{incl} (mm)	0.250	−38.42	3.97
2	78	6084	−37.84		0.375	−35.01	
3	80	6400	−38.06		<u>0.500</u>	−34.46	
4	63	3969	−35.99	r_{hor} (mm)	0.250	−37.16	1.87
5	35	1225	−30.88		<u>0.375</u>	−35.29	
6	81	6561	−38.17		<u>0.500</u>	−35.44	
7	64	4096	−36.12	t_{skin} (mm)	1.0	−38.23	3.58
8	72	5184	−37.15		<u>1.5</u>	−34.64	
9	32	1024	−30.10		<u>2.0</u>	−35.02	
				Empty	level 1	−33.45	3.93
					level 2	−37.38	
					level 3	−37.07	

Table 3. ANOVA results.

Parameter	dF	S_x	Pool	dF_e	S_e	V_x	V_e	F	S_x^*	ρ%	Confidence
r_{incl} (mm)	2	1355	no			677		6.043	1131	33%	86%
r_{hor} (mm)	2	224	yes	2	224	112	112				
t_{skin} (mm)	2	1095	no			547		4.883	871	25%	83%
Empty	2	784	no			392		3.498	560	16%	78%
Total		3458		2	224	1729					
Average							112				

To complete the analysis on the structural behavior of the elementary octahedral cell, the maximum vertical displacement in the model, the displacement at the centre of the upper skin, and the total strain energy absorbed under the applied load of 50 N were extracted from the finite element simulations. These quantities provide insight into the stiffness of the unit cell and its energy absorption capability as a function of the geometric parameters.

Figure 3a shows the values of maximum displacement in the cell and the displacement at the centre of the upper skin in the case of t_{skin} = 1.0 mm, while Figures 3b and 3c report the same quantities for t_{skin} = 1.5 mm and t_{skin} = 2.0 mm, respectively. In order to easily evaluate the various stiffnesses obtained for the nine simulated configurations, Figure 3d presents the force–displacement plots, where the displacement is measured at the centre of the upper skin. Figure 4 shows the values of strain energy for all the runs.

The global stiffness of the cell is given by the contributions of the upper skin, the core and the lower skin. The results show that the stiffness varies significantly across the tested configurations, ranging from approximately 1.4 kN/mm to 5.4 kN/mm. Among the investigated parameters, the skin thickness t_{skin} has an important influence on stiffness. For instance, for configurations with r_{incl} = 0.25 mm, increasing the skin thickness from 1.0 mm to 1.5 mm reduces the central displacement from 0.0347 mm to 0.0285 mm, while a further increase to 2.0 mm provides additional, though less pronounced, stiffening, which results in a displacement of 0.0267 mm. This behaviour is consistent with classical sandwich theory, in which the skins carry most of the bending loads and therefore dominate the stiffness of the panel.

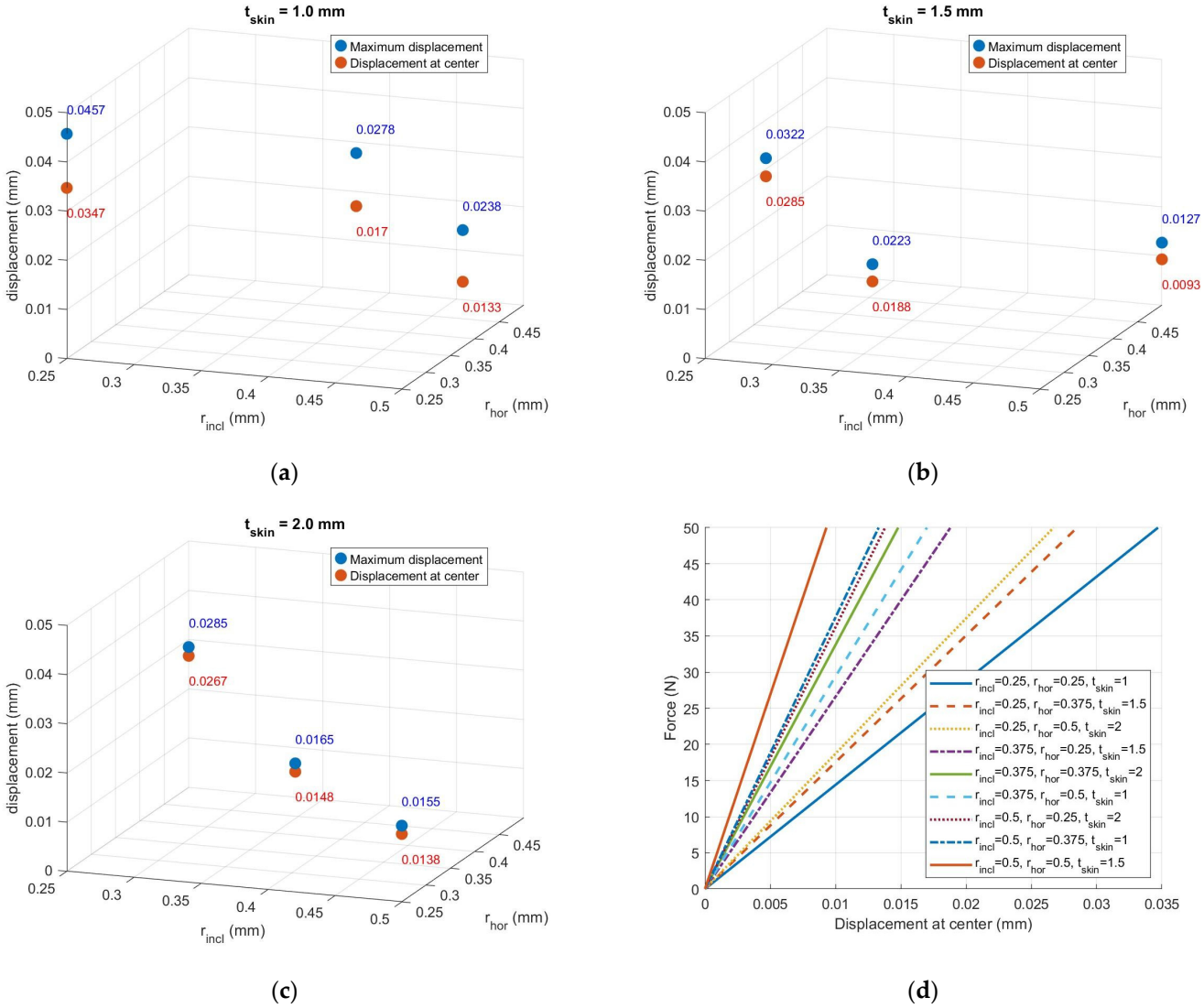

Figure 3. Evaluation of the cell stiffness across the nine runs: (**a**) Displacements for t_{skin} = 1.0 mm; (**b**) Displacements for t_{skin} = 1.5 mm; (**c**) Displacements for t_{skin} = 2.0 mm; (**d**) Force–displacement plots, where the displacement is measured at the centre of the upper skin.

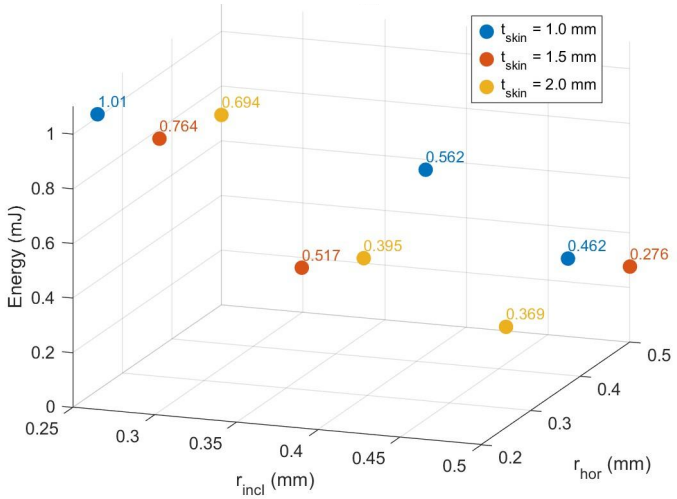

Figure 4. Strain energies for the nine runs.

https://doi.org/10.3390/engproc2026131015

The difference between the maximum displacement and the central displacement provides an indication of the bending deformation of the upper skin, with larger differences corresponding to more pronounced bending. Thinner skins exhibit the largest discrepancy between the two displacement measures, confirming their lower bending stiffness and their tendency to deform. Conversely, thicker skins are more rigid. This effect is particularly evident in runs with t_{skin} = 2.0 mm, where the difference between maximum and central displacement becomes very small.

The radius of the inclined ribs r_{incl} also contributes to the overall stiffness of the cell. Increasing r_{incl} enlarges the effective load-transfer area between the skins and the core, since it increases the axial stiffness of the core and simultaneously limits the deformation of the skins. As a result, configurations with larger inclined ribs exhibit lower displacements and higher stiffness. The effect of r_{incl} is particularly relevant when the skins are relatively thin, as the ribs become the dominant structural elements resisting deformation. When the skins are thicker, the influence of r_{incl} remains beneficial but becomes comparatively less dominant, as the skins themselves provide substantial bending stiffness. The combined contribution of skin thickness and inclined-rib size is pointed out by the achievement of the minimum difference between maximum and central displacements in the configuration with the thickest skins and the largest inclined-rib radius. It is also notable that, for this specific geometry, the horizontal ribs have the smallest cross-section.

The radius of the horizontal ribs r_{hor} was found to have a much smaller influence on stiffness, which is consistent with the Taguchi and ANOVA results obtained for stress analysis. Since the horizontal ribs primarily contribute to core stability, their effect on vertical stiffness of the cell is limited.

It is important to observe that the upper skin in the finite element model is free along its lateral edges, which allows for local bending strains and results in larger displacements compared to a real sandwich panel, where adjacent cells would provide additional lateral support. In a full panel, the continuity of the skins and the presence of neighboring cells would significantly reduce the local curvature of the skin and increase the global stiffness. Therefore, the stiffness values obtained in this study are conservative with respect to the behaviour of a complete anisogrid panel.

The strain energy values obtained from the nine finite element simulations range from 0.276 mJ to 1.01 mJ. The highest strain energy is observed in the configuration with the thinnest skins (t_{skin} = 1.0 mm) and the smallest rib radii (r_{incl} = 0.25 mm, r_{hor} = 0.25 mm), which also corresponds to the largest maximum displacements both in the whole cell and in the centre of the upper skin (0.0457 mm and 0.0347 mm). This behaviour reflects the greater compliance of the structure: thinner skins undergo more pronounced bending strains, and the inclined ribs experience larger axial deformations, resulting in higher elastic strain energy accumulation.

The cross-section of the horizontal ribs has a minor effect on strain energy, while increasing the skin thickness leads to a marked reduction. For instance, when t_{skin} increases from 1.0 mm to 1.5 mm (with r_{incl} = 0.25 mm), the absorbed energy decreases from 1.01 mJ to 0.764 mJ, accompanied by a reduction in maximum displacement from 0.0457 mm to 0.0322 mm. A further increase to t_{skin} = 2.0 mm reduces the strain energy to 0.694 mJ and the maximum displacement to 0.0285 mm. This trend is consistent across all parameter combinations and confirms that the skins significantly affect the stiffness of the cell, thereby controlling both deformation and energy absorption.

The influence of the radius of the inclined ribs r_{incl} is also evident. For example, at t_{skin} = 1.5 mm, increasing r_{incl} from 0.25 mm to 0.50 mm reduces the strain energy from 0.764 mJ to 0.276 mJ and the maximum displacement from 0.0322 mm to 0.0127 mm. This demonstrates that larger inclined ribs enhance the axial stiffness of the load-bearing

members, consequently limiting deformation and reducing the amount of elastic energy in the structure.

Conversely, the radius of the horizontal ribs r_{hor} shows a comparatively minor effect on strain energy. Variations in r_{hor} at fixed values of t_{skin} and r_{incl} lead to changes in strain energy that are significantly smaller than those produced by the other two parameters.

Overall, the combined analysis of stiffness and absorbed energy confirms that the structural behaviour of the octahedral unit cell is governed primarily by the skin thickness and the radius of the inclined ribs. The horizontal ribs play a secondary role under the considered loading conditions. These findings are consistent with the Taguchi and ANOVA analyses carried out on the stress state and provide additional guidance for the design of high-efficiency anisogrid structures.

4. Conclusions

This study investigated the influence of geometric parameters on the von Mises stress distribution in octahedral unit cells of anisogrid sandwich panels through finite element analysis combined with the Taguchi method and ANOVA. To provide a more comprehensive analysis on the mechanical response, the global stiffness and strain energy were also assessed from the finite element simulations.

The radius of the inclined ribs and the thickness of the skins were found to contribute significantly to the structural behavior of the cell. The Taguchi analysis also identified an "empty" parameter with statistical relevance on stress state. The "empty" factor may represent additional influences such as material properties, load conditions or volume of the cell. The identification of this "empty" parameter as significant highlights the need for further investigation into other design variables that may influence structural performance.

Overall, the methodology employed in this work provides a robust framework for evaluating and optimizing anisogrid structures, supporting the design of lightweight, high-performance components. The findings suggest that targeted geometric refinement can lead to substantial improvements in structural efficiency.

Author Contributions: Conceptualization, E.V.A. and S.B.; methodology, E.V.A. and S.B.; software, E.V.A. and S.B.; validation, E.V.A. and S.B.; formal analysis, E.V.A. and S.B.; investigation, E.V.A. and S.B.; resources, E.V.A. and S.B.; data curation, E.V.A. and S.B.; writing—original draft preparation, E.V.A.; writing—review and editing, S.B.; visualization, E.V.A. and S.B.; supervision, E.V.A. and S.B.; project administration, E.V.A.; funding acquisition, E.V.A. All authors have read and agreed to the published version of the manuscript.

Funding: The activity was conducted within the project "Innovative multiphysical approach to aerospace metamaterials design"—PRIN 2022 PNRR (DD MUR n.1409 del 14-9-2022), founded by the European Union—NextGenerationEU—M4, C2, 1.1.—CUP: F53D23009910001.

Institutional Review Board Statement: Not applicable.

Informed Consent Statement: Not applicable.

Data Availability Statement: Data are available upon request.

Conflicts of Interest: The authors declare no conflicts of interest.

References

1. Vasiliev, V.V.; Barynin, V.; Razin, A.F. Anisogrid lattice structures—Survey of development and application. *Compos. Struct.* **2001**, *54*, 361–370. [CrossRef]
2. Morozov, E.V.; Lopatin, A.V.; Shatov, A.V.; Kazantsev, Z.A. Composite anisogrid lattice toroidal shell: Application to a load-carrying rim of the spacecraft reflectarray antenna. *Compos. Struct.* **2024**, *331*, 117860. [CrossRef]
3. Morozov, E.V.; Lopatin, A.V.; Khakhlenkova, A.A. Finite-element modelling, analysis and design of anisogrid composite lattice spoke of an umbrella-type deployable reflector of space antenna. *Compos. Struct.* **2022**, *286*, 115323. [CrossRef]

4. Kusni, M.; Hadi, B.K.; Gunawan, L.; Syamsudin, H. Development of Anisogrid Lattice Composite Structures for Fighter Wing Applications. *Int. J. Aerosp. Eng.* **2024**, *2024*, 6667586. [CrossRef]
5. Nesterov, V.A.; Nikishev, A.A. Buckling and stiffness analysis of a composite anisogrid conical shell with a fixed small base. *Sib. Aerosp. J.* **2025**, *26*, 94–106. [CrossRef]
6. Totaro, G.; Gürdal, Z. Optimal design of composite lattice shell structures for aerospace applications. *Aerosp. Sci. Technol.* **2009**, *13*, 157–164. [CrossRef]
7. Gentili, S.; Greco, L.; Mancia, T.; Simoncini, M. Influence of geometric parameters on buckling behavior of 3D printed anisogrid structures. *Key Eng. Mater.* **2022**, *926*, 115–121. [CrossRef]
8. Jeon, M.-H.; Kim, I.-G.; Woo, K. Progressive failure analysis of anisogrid cylindrical composite lattice structure with manufacturing defects. *Compos. Struct.* **2023**, *321*, 117237. [CrossRef]
9. Belardi, V.G.; Fanelli, P.; Vivio, F. Structural analysis and optimization of anisogrid composite lattice cylindrical shells. *Compos. Part B Eng.* **2018**, *139*, 203–215. [CrossRef]
10. Belardi, V.G.; Fanelli, P.; Vivio, F. Design, analysis and optimization of anisogrid composite lattice conical shells. *Compos. Part B Eng.* **2018**, *150*, 184–195. [CrossRef]
11. Sun, F.; Lai, C.; Fan, H. Failure mode maps for composite anisogrid lattice sandwich cylinders under fundamental loads. *Compos. Sci. Technol.* **2017**, *152*, 149–158. [CrossRef]
12. Fan, H.L.; Meng, F.H.; Yang, W. Sandwich panels with Kagome lattice cores reinforced by carbon fibers. *Compos. Struct.* **2007**, *81*, 533–539. [CrossRef]
13. Li, S.; Jin, F.; Zhang, W.; Meng, X. Research of hail impact on aircraft wheel door with lattice hybrid structure. *J. Phys. Conf. Ser.* **2016**, *744*, 012102.
14. Xue, B.; Peng, Y.-X.; Ren, S.-F.; Liu, N.-N.; Zhang, Q. Investigation of impact resistance performance of pyramid lattice sandwich structure based on SPH-FEM. *Compos. Struct.* **2021**, *261*, 113561. [CrossRef]
15. Hou, S.; Li, T.; Jia, Z.; Wang, L. Mechanical properties of sandwich composites with 3D-printed auxetic and non-auxetic lattice cores under low velocity impact. *Mater. Des.* **2018**, *160*, 1305–1321.
16. Lei, H.; Li, C.; Meng, J.; Zhou, H.; Liu, Y.; Zhang, X.; Wang, P.; Fang, D. Evaluation of compressive properties of SLM-fabricated multi-layer lattice structures by experimental test and μ-CT-based finite element analysis. *Mater. Des.* **2019**, *169*, 107685. [CrossRef]
17. Nasrullah, A.I.H.; Santosa, S.P.; Dirgantara, T. Design and optimization of crashworthy components based on lattice structure configuration. *Structures* **2020**, *26*, 969–981. [CrossRef]
18. Arcieri, E.V.; Baragetti, S. Finite element analysis of anisogrid lattice structures. *Procedia Struct. Integr.* **2026**, *80*, 130–135. [CrossRef]
19. Condra, L.W. *Reliability Improvement with Design of Experiments*, 1st ed.; Marcel Dekker Inc.: New York, NY, USA, 1993; pp. 1–300.